Materials Horizons

Accepted Manuscript

ROYAL SOCIETY OF CHEMISTRY

rsc.li/materials-horizons

Journal Name

RSCPublishing

COMMUNICATION

Modulate Hybrid Organic–Perovskite Photovoltaic Performance by Controlling the Excited Dynamics of Fullerenes

Cite this: DOI: 10.1039/x0xx00000x

Received 00th January 2012,
Accepted 00th January 2012

DOI: 10.1039/x0xx00000x

www.rsc.org/

Chang-Zhi Li,[a] Po-Wei Liang,[a] Dana B. Sulas,[b] Phu D. Nguyen,[b] Xiaosong Li,[b] David S. Ginger,[b] Cody W. Schlenker,[b] and Alex K.-Y. Jen [a, b,*]

We present a synergistic approach to modulate organic-perovskite interfaces and their photovoltaic behaviors by tuning the properties of n-contact fullerene layered atop of perovskite. Fullerenes with excited charge transfer are found to not only suppress fullerene photoluminescence, but also enhance molecular polarization and transport capabilities. This results in optimized perovskite-fullerene contact.

Methyl ammonium lead halide perovskites have recently gained popularity as solution-processable materials for highly efficient photovoltaics (PVs), with power conversion efficiencies (PCEs) rising from 3.8% to over 20% within last five years.[1-5] State-of-the-art perovskite photovoltaics perform well with an inorganic/organic p-i-n planar heterojunction (PHJ) architecture, in which organic layers (p or n-layer) interface with the perovskite (i-layer) (Scheme 1).[5-11] One intriguing, yet less explored, question is how the properties of the organic-perovskite heterointerface affect the operation of photovoltaics. Ideally, efficient device operation requires photo-generated charge carriers to be extracted from the perovskite into molecular orbitals of organic semiconductors with only minimal energy and carrier losses.[12-14] Proper charge selective contacts are vital to realize this.[15] Low charge carrier mobilities and carrier densities in organic semiconductors may limit efficient charge extraction at the perovskite/organic interface. For instance, commonly used electron extraction layers, such as non-polar PCBM,[16] typically have mobilities around 10^{-2} $cm^2V^{-1}s^{-1}$ in comparison to the organohalide lead perovskite, which exhibits very high carrier mobility ~ 30 $cm^2V^{-1}s^{-1}$ and photoconductivities up to 10^{-2} Scm^{-1}.[17-20] In addition, the search for new electron-selective contacts is also largely motivated by the desire to introduce mild processing materials for device fabrications.

In this work, we present a synergistic approach to modulate organic-perovskite interfaces and their photovoltaic behaviours by tuning the properties of n-contact fullerene layered atop of perovskite (Scheme 1). New fullerenes are functionalized with triphenylamine (TPA) moieties and used as n-layer contacts to $CH_3NH_3PbI_{3-x}Cl_x$ perovskite for PHJ PVs. The resulting photovoltaic devices employing these fullerenes show correlations between increasing photocurrent and increasing electron-donating character of the TPA. The integrative computational and spectroscopic studies on these chosen materials suggest that the increase of CT probabilities between the fullerene and TPA competes with singlet exciton decay and counteracts the excitonic nature associated with regular organic semiconductors. Accordingly, fullerenes exhibiting CT characteristics simultaneously improve molecular polarization, carrier densities, and charge transport capabilities under light excitation, leading to improved photocurrent and performance of perovskite PVs when the perovskite layer is interfaced with these fullerenes.

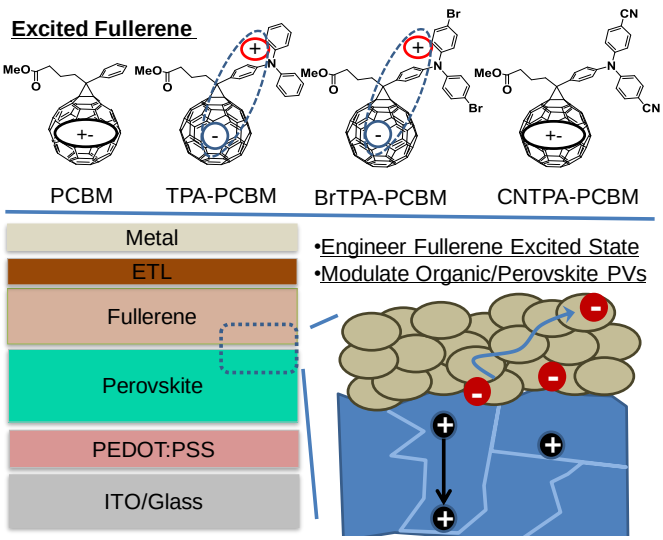

Scheme 1. Schematic representation of the excited CT characters of four chosen fullerene derivatives that are layered atop of $CH_3NH_3PbI_{3-x}Cl_x$ perovskite planar heterojunction PVs.

Scheme 1 shows the molecular structures of the fullerenes we studied, PCBM, TPA-PCBM, BrTPA-PCBM and CNTPA-PCBM respectively, where we replace the phenyl group of $PC_{61}BM$ with functional TPA moieties (Supporting Information, SI and Fig. S1 & S2).[21, 22] The resulting fullerenes can be easily processed through common organic solvents, such as chloroform, toluene,

chlorobenzene, and o-dichlorobenzene. TPA-$PC_{61}BM$ was previously demonstrated to improve the thermal stability of BHJ solar cells with P3HT due to its low crystallinity and good electron mobility.[22] In the present study, we examine how the fine-tuning of TPA moieties affects the operation of fullerene-perovskite junctions and their photovoltaic behaviours. By increasing the electron-withdrawing abilities of the TPA substituents (H < Br << CN), we effectively tune the donating strength of TPA moieties and regulate CT between TPA and the fullerene cage (i.e. electron localization on the fullerene and hole localization on the TPA). These changes result in a modulation of PV performance.

We first examine these modified fullerenes as n-layer contacts atop of the $CH_3NH_3PbI_{3-x}Cl_x$ perovskite absorber, and we find ~99% quenching of the perovskite photoluminescence intensity (Fig. S3), suggesting effective charge transfer from the perovskite to the fullerene layer. We employ a planar heterojunction (PHJ) solar cell architecture to evaluate their photovoltaic performance in the configuration of ITO/PEDOT:PSS (~ 30 nm)/perovskite (~ 250 nm)/fullerene (~ 55 nm)/Bis-C_{60} (10 nm)/Ag (150 nm).[6] The purpose of using relatively thin perovskite from one-step process is to provide easier probing of the effect of fullerene functionalities on the photovoltaic behaviours of organic/perovskite PHJ solar cells. Bis-C_{60} interfacial layer is used to improve the interfacial contact between n-layer fullerene and silver cathode (please see SI for Bis-C_{60} structure).[23-25] Fig. 1 and Table 1 summarize the current-voltage characteristics, external quantum efficiency (EQE), and overall perovskite device performance with the four different fullerene n-layers under 1 sun AM 1.5 simulated solar irradiation.

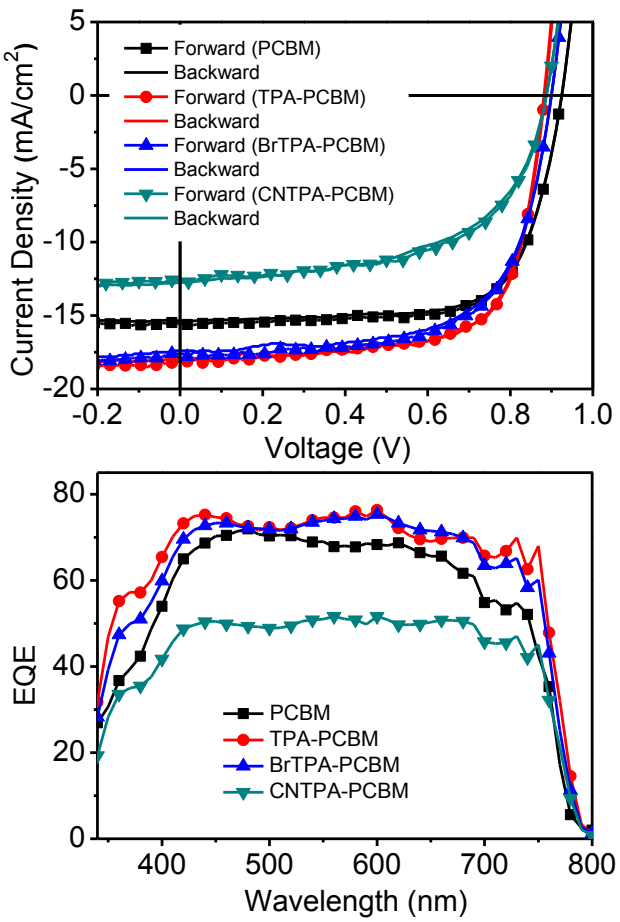

Fig. 1 (a) Current density−voltage curves by reverse and forward sweeping at the rate of 1 V/s (b) EQE spectra for the different fullerene based solar cells measured under AM1.5G illumination at 100 mW/cm^2.

Table 1. Characteristics of photovoltaic Devices [a]

	PCE (%)	*V_{oc}/V*	*FF*	*J_{sc}/mAcm^{-2}*
PCBM	9.88 ±0.37	0.90 ±0.01	0.68 ±0.02	15.70 ±0.42
TPA-	10.87 ±0.51	0.88 ±0.02	0.69 ±0.03	17.71 ±0.54
BrTPA-	10.20 ±0.38	0.89 ±0.02	0.67 ±0.05	17.18 ±0.43
CNTPA-	5.60 ±0.81	0.90 ±0.02	0.48 ±0.06	13.76 ±0.37

[a] The error bars represent the standard deviation of 25 devices.

The proof-of-concept device employing TPA-PCBM contact layer exhibits a promising averaged PCE of 10.87 ± 0.51 % with a much improved J_{SC} of 17.71 ± 0.54 mA cm^{-2} , which represents a ~ 13% enhancement of Jsc compared to that of the standard $PC_{61}BM$ device (*Jsc*, 15.70 ± 0.42 mA cm^{-2} and PCE of 9.88 ± 0.37%). This notable current enhancement is consistent with the improved EQE over the entire spectral range shown in Fig. 1b. The TPA-PCBM based devices reach photon-to-electron conversion ~ 80% of external quantum efficiencies (EQE) in broad range of spectra that is comparable to that of state-of-art perovskite devices reported so far.[26] A similar current enhancement from BrTPA-PCBM, with higher J_{SC} and EQE as well as decent PCE of 10.20 ± 0.38 % (V_{OC}: 0.89 V; J_{SC}: 17.18 mAcm^{-2}; FF: 0.67). Note that a severe decrease of performance is observed from the CNTPA-PCBM device with a PCE of 5.60 ± 0.81 % due to large drop of J_{SC} (13.76 ± 0.37 mAcm^{-2}) and FF (0.48 ± 0.06). CNTPA-PCBM device also show the lowest EQE among four fullerenes. The calculated Jsc values ($PC_{61}BM$ of 15.6 mAcm^{-2}; TPA-$PC_{61}BM$ of 17.6 mAcm^{-2}; BrTPA-$PC_{61}BM$ of 17.2 mAcm^{-2} and CNTPA-$PC_{61}BM$ of 12.0 mAcm^{-2}) are estimated from the integration of EQE spectra match well with those obtained from the J−V measurements. In addition, devices employing no fullerene n-contact layers between perovskite and Bis-C_{60} interfacial layer fail to yield normal operations. More importantly, we observe the negligible hysteresis in these devices with both reverse and forward voltage sweep (Fig. 1a&S4), which is a sharp contrast to the severe hysteresis reported in many types of perovskite PVs. Detail studies along this direction are in progress. We expect that the organic contacts and thin-perovskite layer based PHJ architecture used here allow suppressing charge trapping to eliminate photocurrent hysteresis.[9, 14, 26, 27]

It is interesting to note that photovoltaic devices employing fullerenes with electron-donating TPA moieties (i.e., TPA-$PC_{61}BM$ and BrTPA-$PC_{61}BM$) show notable enhancement of photocurrent and EQE compared to those derived from using $PC_{61}BM$. On the other hand, devices employing CNTPA-$PC_{61}BM$, in which the nitrile group suppresses TPA electron-donating character, show poor photocurrent and low overall device efficiency. This suggests some correlations between increasing photocurrent and increasing electron-donating character of the TPA.

Cyclic voltammetry (Fig. 2 and Table 2) shows similar reversible reduction peaks for all species, with the first reduction potential, $E_{1/2}^{red\ 1}$ values being -587 mV ($PC_{61}BM$), -596 mV (TPA-$PC_{61}BM$), -585 mV (BrTPA-$PC_{61}BM$) and -568 mV (CNTPA-$PC_{61}BM$). These indicate fullerene LUMO energetics show negligible variation in the small range of 30 meV (Table 2). It suggests no extra barrier is introduced for extracting electron from perovskite to fullerene when replacing the phenyl group of $PC_{61}BM$ with TPA moieties. Reversible oxidative peaks are detected for TPA-$PC_{61}BM$ (1094 mV) and BrTPA-$PC_{61}BM$ (1198 mV) that are similar to TPA itself (1052 mV). The oxidative peaks are absent for

$PC_{61}BM$ and CNTPA-$PC_{61}BM$ due to the suppressed electron-donating character of CNTPA pendent.

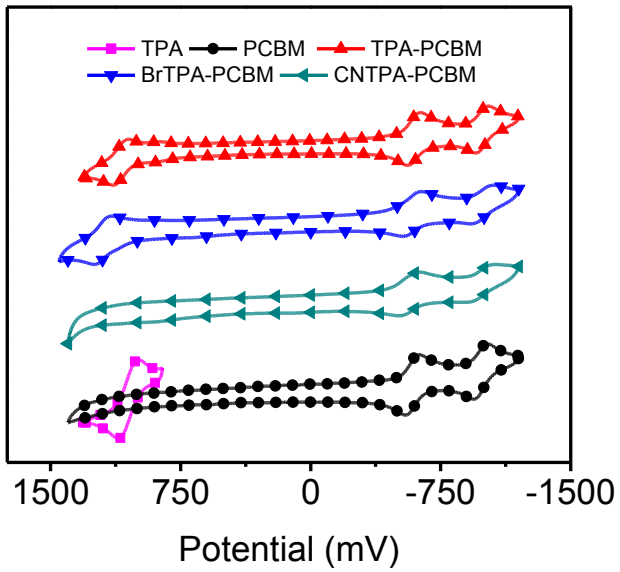

Fig. 2 Cyclic voltammogram of four different fullerenes measured in dichloromethane solution.

Note that TPA-PC61BM and BrTPA-PC61BM exhibit not only the existence of oxidative peaks (electron donating characters) but also improved photocurrent and EQE in photovoltaic devices, suggesting the photovoltaic enhancement instead arises from variation in charge localization. We direct our attention to the electronic structure of these new fullerene derivatives. We model the frontier molecular orbitals (HOMO and LUMO), excited states, and dipole moment using density functional theory (DFT) (See also SI, Fig. 3 & S5). Fig. 3 shows the charge distribution of the lowest singlet excited state of the four fullerenes, which can be divided into two categories: fullerenes with intramolecular CT (hereafter as CT-fullerenes) and fullerenes without CT character (NCT-fullerenes). CT-fullerenes (TPA-$PC_{61}BM$ and BrTPA-$PC_{61}BM$) show spatial separation of the hole (cyan) on TPA moieties, and electron (blue) on the fullerene cage. These CT-fullerenes exhibit exceptionally large excited state dipole moments (E_D) of approximately 35 Debye, which is an order of magnitude higher than their ground state dipole moments (G_D) (Table 2). However, the NCT-fullerenes ($PC_{61}BM$ and CNTPA-$PC_{61}BM$) display negligible changes between E_D and G_D (Table 2), suggesting that the excited state likely consists of a bound electron-hole pair located on the fullerene cage.

Fig. 4a shows PL spectra for a dilute solution of each fullerene in benzonitrile (dielectric constant, $\varepsilon = 26.0$), and Fig. 4b shows the corresponding PIA spectra. The PL spectral shape remains the same for all fullerenes, and the spectra match previous literature reports for C_{60} singlet emission.[28] We observe quenched emission for CT-fullerenes (TPA-$PC_{61}BM$ and BrTPA-$PC_{61}BM$) compared to NCT-fullerenes ($PC_{61}BM$ and CNTPA-$PC_{61}BM$). The PIA spectra for NCT fullerenes both exhibit strong peaks at 780 nm, which has been previously assigned as the triplet absorption band.[28, 29] In contrast, this triplet absorption band is strongly suppressed in the CT fullerenes. Together, these data suggest that the intramolecular CT state forms faster than the fullerene PL decay (~ 1.4 ns), or intersystem crossing times (> 1.4 ns for $PC_{61}BM$).[30]

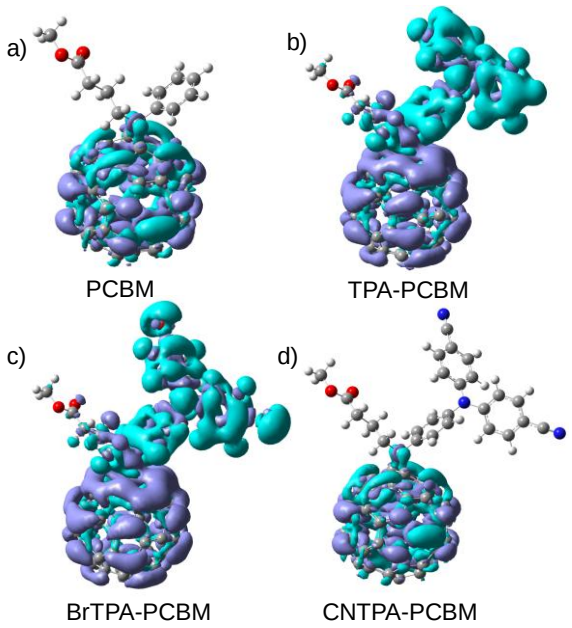

Fig. 3 Frontier orbital charge density distribution shown for lowest excited fullerene (color code: cyan for electron while light blue represents the hole).

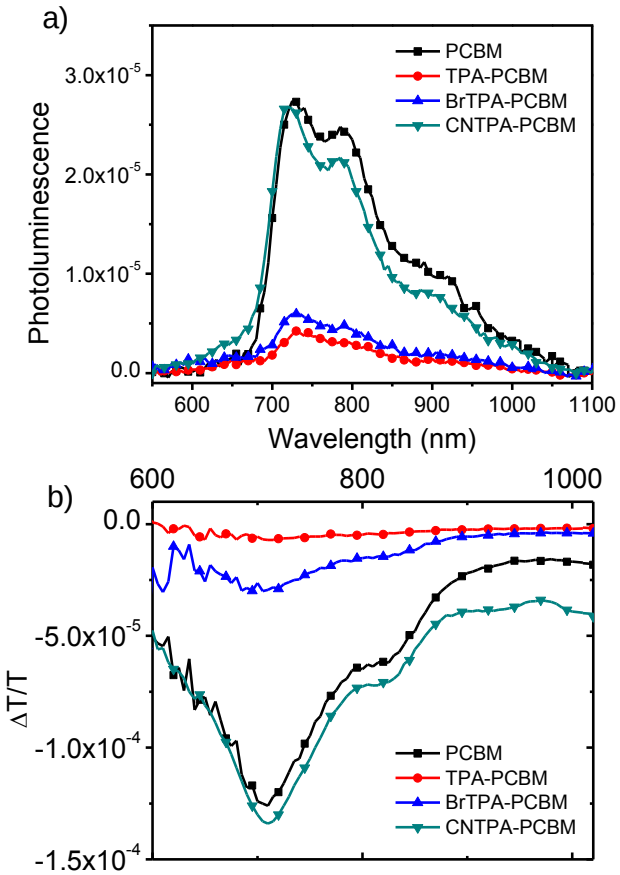

Fig. 4 (a) Photoluminescence and (b) photoinduced absorption spectra of diluted fullerene solutions in anaerobic benzonitrile (0.17 mg/mL).

Journal Name

RSCPublishing

COMMUNICATION

Table 2. Dipole, energy levels and charge mobility for the studied fullerenes.

Compounds	G_D *(Debye)*	E_D *(Debye)*	$E_{1/2}^{OX1}$ *(mV)*	$E_{1/2}^{Red1}$ *(mV)*	$E_{1/2}^{Red2}$ *(mV)*	*HOMO*[a] *(meV)*	*LUMO*[a] *(meV)*	J_{ph}/J_o[b]	*FET(μ)* $(cm^2V^{-1}s^{-1})$
PCBM	3.60	4.49	N.A.	-587	-979	N.A.	-3698	6.11	0.084
TPA-PCBM	3.94	37.32	1094	-596	-989	5379	-3689	36.22	0.036
BrTPA-PCBM	3.26	36.46	1198	-585	-993	5483	-3700	40.67	0.049
CNTPA-PCBM	6.13	5.87	N.A.	-568	-937	N.A.	-3717	15.35	0.019

[a] The energy levels are determined from the equation of $E_{HOMO} = -(E_{1/2}^{OX1} - E_{Fc/Fc+} + 4800)$ (meV) and $E_{LUMO} = -(E_{1/2}^{Red1} - E_{Fc/Fc+} + 4800)$ (meV), respectively. [b] Averaged J_{ph}/J_o ratio of ITO/ZnO/fullerene/Ca/Al devices (V_{eff} from 0 V to 0.8 V).

We further study how the excited CT between fullerene and TPA affects electron transport of n-contact layer, finding the enhanced photoexcited charge transport in CT-fullerenes. By evaluating the change in current densities measured in the dark (J_o) and under 1 sun AM1.5 solar irradiation (J_{ph}) in ITO/ZnO/fullerene/Ca/Al devices, we find that the trend for J_{ph}/J_o enhancement correlates with the increased ratio in dipole moment E(D)/E(G) (Fig. 5 and Table 2).

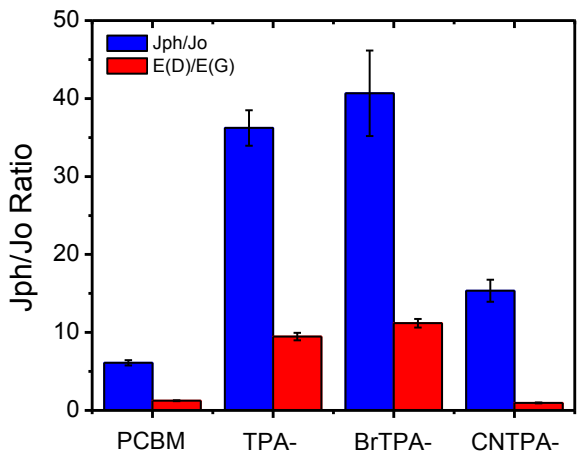

Fig. 5 Plots for current density ratio, J_{ph}/J_o under light and dark along with the calculated dipole change, E(D)/E(G).

CT-fullerenes (TPA-PC_{61}BM and BrTPA-PC_{61}BM) exhibit large enhancement in J_{ph}/J_o (>36 times), while the NCT-fullerenes, PC_{61}BM (6.1 times) and CNTPA-PC_{61}BM (15.3 times) show less prominent change in J_{ph}/J_o ratio. Although PC_{61}BM itself exhibits relatively better field-effect transistor (FET) and space charge limited current (SCLC) mobilities measured under dark (Fig. S6, S7 and S8), the CT-fullerene generates the spatially separated hole on TPA moieties and electron on the fullerene cage under excitation, a polarized state that results in the optimized inorganic/fullerene interfacial contact and the enhanced fullerene photoconductive effect, especially carrier densities, thus boost photocurrent and EQE of perovskite PHJ PVs.

Conclusions

In conclusion, we combine new fullerene synthesis, computation, spectroscopy, and device characterization to demonstrate that controlled charge transfer between fullerene and functional addends allows us to modulate PV performance. Interestingly, these devices do not show the common hysteresis effect observed in many perovskite PVs, which indicate that organic contacts used here can mitigate the perovskite defect states and minimize photocurrent hysteresis in organic/perovskite PHJ solar cell. Fullerenes with intramolecular CT characteristics improve molecular polarization, carrier density, and transport upon excitation, which in turn improve the device operation of PHJ perovskite PVs. It provides a useful model to uncover the fundamental factors to optimize organic-inorganic hybrid electronics.

Experimental section

All reactions dealing with air- or moisture-sensitive compounds were carried out using standard Schlenk technique. P-tosylhydrazides were synthesized according to literature methods.[21, 22]

Synthesis of Functional Fullerene: To the dry pyridine (5 mL) solution of methyl-4-(diphenylamino)phenylbenzoylbutyrate tosylhydrazone (0.6 mmol), sodium methoxide (0.6 mmol) were added in one potion under an atmosphere of Argon. The mixture was stirred at room temperature for 10 mins. [60]fullerene (0.42 mmol) in anhydrous ODCB (50 mL) was then transferred to the resulting suspension. The reaction mixture was heated to 75 ^oC for 40 hours under argon, and then reflux for additional 5 hours. After cooling to room temperature, the solution was then precipitated with methanol. Chromatograph purification on a silica gel column to give product. TPA-PC_{61}BM and BrTPA-PC_{61}BM were purified with the eluent of toluene/hexane mixture (first 1/4, then toluene/hexane = 1/1). CNTPA-PC61BM was purified with the eluent of toluene, and then toluene/EA. Spectral data for TPA-PC_{61}BM (36% yield) was identical to the reported one.[22] BrTPA-PCBM (40% yield), ^{1}H NMR ($CDCl_3$, δ): 2.22 (m, 2H), 2.56 (t, J = 7 Hz, 2H), 2.90 (m, 2H), 3.70 (s, 3H), 7.04 (d, J = 9 Hz, 4H), 7.16 (d, J = 8.5 Hz, 2H), 7.41 (d, J = 9 Hz, 4H), 7.76 (d, J = 9 Hz, 2H); ^{13}C NMR ($CDCl_3$, δ): 22.96, 34.07, 34.41, 51.80, 52.22, 80.49, 116.84, 106.99, 107.06, 119.28, 123.12, 123.41, 126.74, 131.34, 133.12, 133.53, 138.02, 138.51, 141.27, 141.48, 142.61, 142.62, 142.66, 142.73, 143.44, 143.50, 143.64, 144.27, 144.57, 144.92, 145.01, 145.17, 145.26, 145.30, 145.56, 145.60, 145.65, 145.69, 145.72, 146.32, 146.63, 147.14, 148.27, 149.31, 173.99; ESI HR-Mass ($C_{84}H_{21}Br_2NO_2$) calcd, 1232.9934;

found, 1132.9887. CNTPA-PCBM (30% yield), ^{1}H NMR ($CDCl_3$, δ): 2.23 (m, 2H), 2.58 (t, J = 7.5 Hz, 2H), 2.93 (m, 2H), 3.71 (s, 3H), 7.20 (d, J = 8.5 Hz, 4H), 7.28 (d, J = 9 Hz, 4H), 7.60 (d, J = 9 Hz, 4H), 7.92 (d, J = 9 Hz, 2H); ^{13}C NMR ($CDCl_3$, δ): 22.95, 33.98, 34.31, 51.52, 52.87, 80.12, 106.92, 106.99, 107.06, 119.28, 123.36, 123.41, 124.66, 124.70, 126.96, 127.01, 133.59, 133.66, 134.92, 134.94, 134.97, 135.00, 137.85, 138.59, 141.36, 141.58, 142.54, 142.62, 142.73, 143.51, 143.58, 143.61, 143.70, 144.30, 144.68, 145.00, 145.08, 145.22, 145.25, 145.34, 145.52, 145.65, 145.73, 145.76, 145.80, 146.20, 147.91, 149.02, 150.54, 173.97; ESI HR-Mass ($C_{86}H_{21}N_3O_2$) calcd, 1127.1628; found, 1127.1639.

Perovskite PV Fabrication and Characterization: The devices were fabricated in the configuration of ITO/PEDOT:PSS/$CH_3NH_3PbI_{3-x}Cl_x$/fullerene/fullerene surfactant (C_{60}-bis)/Ag. ITO (15 ohm/sq) glass substrates were cleaned sequentially with detergent and deionized water, acetone, and isopropanol under sonication for 10 minutes. After drying under a N_2 stream, substrates were further cleaned by a plasma treatment for 20 s. PEDOT:PSS (Baytron P VP Al 4083, filtered through a 0.45 μm nylon filter) was first spin-coated onto the substrates at 5k rpm for 30 s and annealed at 150 ℃ for 10 min in air. Methylammonium iodide (MAI) was synthesis by reacting methylamine (33 wt% in absolute ethanol, Aldrich) and hydroiodic acid (57 wt% in water with 1.5% hypophosphorous acid, Alfa Aesar) at 2:1 ratio in ethanol at 0 ℃ for 2 h with stirring under nitrogen. After reaction, MAI precipitation was recovered by rotary evaporation at 40 ℃ and then dissolved in ethanol. The pure MAI was recrystallized from diethyl ether and dried at 50 ℃ in a vacuum oven for 24 h. To prepare the perovskite precursor solution, MAI and lead chloride ($PbCl_2$, Aldrich) powder were mixed in anhydrous dimethylformamide (DMF, Aldrich) at a molar ratio of 3:1 with 1wt% of 1,8-Diiodooctane (DIO, Aldrich) with respect to perovskite weight. Perovskite precursor were then deposited through spin-coating at 6k rpm for 45 s (300-500 nm thickness) and then annealed at 90 ^{o}C for 2~3 hours. Afterward, the PCBM/TPA-PCBM/BrTPA-PCBM/CNTPA-PCBM (15 mg/mL in chloroform) and C_{60}-bis surfactant (2 mg/mL in isopropyl alcohol) were then sequentially deposited by spin coating at 1k rpm for 60 s and 3k rpm for 60 s, respectively. Silver electrodes with a thickness of 150 nm were finally evaporated under high vacuum (<2 x 10^{-6} Torr) through a shadow mask. The device area is defined as 3.14 mm^2. All the *J-V* curves in this study were recorded using a Keithley 2400 source meter unit. The device photocurrent was measured under AM1.5 illumination condition at intensity of 100 mW cm^{-2}. The illumination intensity of the light source was accurately calibrated with a standard Si photodiode detector equipped with a KG-5 filter, which can be traced back to the standard cell of the National Renewable Energy Laboratory (NREL). The EQE spectra performed here were obtained from an IPCE setup consisting of a Xenon lamp (Oriel, 450 W) as the light source, a monochromator, a chopper with a frequency of 100Hz, a lock-in amplifier (SR830, Stanford Research Corp), and a Si-based diode (J115711-1-Si detector) for calibration

Acknowledgements

We acknowledge the DOE SunShot (DE-EE0006710), the AOARD (FA2386–11–1–4072), the ONR (N00014-14-1-0170 and N00014-14-1-246), the NSF (CHE-1265945 & DMR-1215753) and the Boeing Foundation for financial support. D.B.S. thanks NSF Graduate Research Fellowship (No. 2013118402) support. We thank Dr. Yue Zang and Dr. Jiang Huang for the SCLC mobility measurements, and Mr. Namchul Cho for FET mobility measurements.

Notes and references

[a]Department of Materials Science and Engineering, University of Washington, Seattle, WA 98195, USA.
[b]Department of Chemistry, University of Washington, Seattle, WA 98195, USA

Electronic Supplementary Information (ESI) available: experimental details, and supplementary scheme and figures referred in the text. See DOI: 10.1039/c000000x/

References

1. A. Kojima, K. Teshima, Y. Shirai and T. Miyasaka, *J. Am. Chem. Soc.*, 2009, **131**, 6050.
2. H. Zhou, Q. Chen, G. Li, S. Luo, T.-b. Song, H.-S. Duan, Z. Hong, J. You, Y. Liu and Y. Yang, *Science*, 2014, **345**, 542.
3. H. J. Snaith, *J. Phys. Chem. Lett.*, 2013, **4**, 3623.
4. N.-G. Park, *J. Phys. Chem. Lett.*, 2013, **4**, 2423.
5. Q. Wang, Y. Shao, Q. Dong, Z. Xiao, Y. Yuan and J. Huang, *Energy. Environ. Sci.*, 2014, **7**, 2359.
6. P.-W. Liang, C.-Y. Liao, C.-C. Chueh, F. Zuo, S. T. Williams, X.-K. Xin, J. Lin and A. K. Y. Jen, *Advanced materials*, 2014, **26**, 3748.
7. J. M. Ball, M. M. Lee, A. Hey and H. J. Snaith, *Energy. Environ. Sci.*, 2013, **6**, 1739.
8. O. Malinkiewicz, A. Yella, Y. H. Lee, G. M. Espallargas, M. Graetzel, M. K. Nazeeruddin and H. J. Bolink, *Nat. Photonics*, 2014, **8**, 128.
9. Q. Lin, A. Armin, R. C. R. Nagiri, P. L. Burn and P. Meredith, *Nat. Photonics*, 2015, **9**, 106.
10. Y. Guo, C. Liu, K. Inoue, K. Harano, H. Tanaka and E. Nakamura, *J. Mater. Chem. A*, 2014, **2**, 13827.
11. O. Malinkiewicz, C. Roldán-Carmona, A. Soriano, E. Bandiello, L. Camacho, M. K. Nazeeruddin and H. J. Bolink, *Adv. Energy Mater.*, 2014, **4**, 1400345.
12. A. Abrusci, S. D. Stranks, P. Docampo, H.-L. Yip, A. K. Y. Jen and H. J. Snaith, *Nano. Lett.*, 2013, **13**, 3124.
13. M.-F. Lo, Z.-Q. Guan, T.-W. Ng, C.-Y. Chan and C.-S. Lee, *Adv. Funct. Mater.*, 2015, **25**, 1213.
14. K. Wojciechowski, S. D. Stranks, A. Abate, G. Sadoughi, A. Sadhanala, N. Kopidakis, G. Rumbles, C.-Z. Li, R. H. Friend, A. K. Y. Jen and H. J. Snaith, *ACS Nano.*, 2014, **8**, 12701.
15. E. J. Juarez-Perez, M. Wuβler, F. Fabregat-Santiago, K. Lakus-Wollny, E. Mankel, T. Mayer, W. Jaegermann and I. Mora-Sero, *J. Phys. Chem. Lett.*, 2014, **5**, 680.
16. C.-Z. Li, C.-C. Chueh, H.-L. Yip, J. Zou, W.-C. Chen and A. K. Y. Jen, *J. Mater. Chem.*, 2012, **22**, 14976.
17. T. Leijtens, S. D. Stranks, G. E. Eperon, R. Lindblad, E. M. J. Johansson, I. J. McPherson, H. Rensmo, J. M. Ball, M. M. Lee and H. J. Snaith, *ACS Nano.*, 2014, **8**, 7147.
18. G. Xing, N. Mathews, S. Sun, S. S. Lim, Y. M. Lam, M. Grätzel, S. Mhaisalkar and T. C. Sum, *Science*, 2013, **342**, 344.

19. S. D. Stranks, G. E. Eperon, G. Grancini, C. Menelaou, M. J. P. Alcocer, T. Leijtens, L. M. Herz, A. Petrozza and H. J. Snaith, *Science*, 2013, **342**, 341.
20. P. Gao, M. Gratzel and M. K. Nazeeruddin, *Energy. Environ. Sci.*, 2014, **7**, 2448.
21. C.-Z. Li, S.-C. Chien, H.-L. Yip, C.-C. Chueh, F.-C. Chen, Y. Matsuo, E. Nakamura and A. K. Y. Jen, *Chem. Comm.*, 2011, **47**, 10082.
22. Y. Zhang, H.-L. Yip, O. Acton, S. K. Hau, F. Huang and A. K. Y. Jen, *Chem. Mater.*, 2009, **21**, 2598.
23. K. M. O'Malley, C.-Z. Li, H.-L. Yip and A. K. Y. Jen, *Adv. Energy Mater.*, 2012, **2**, 82.
24. C.-Z. Li, C.-Y. Chang, Y. Zang, H. X. Ju, C.-C. Chueh, P. W. Liang, N. Cho, D. S. Ginger and A. Y. K. Jen, *Adv. Mater.*, 2014, **26**, 6262.
25. C.-Z. Li, C.-C. Chueh, H.-L. Yip, F. Ding, X. Li and A. K. Y. Jen, *Adv. Mater.*, 2013, **25**, 2457.
26. W. Nie, H. Tsai, R. Asadpour, J.-C. Blancon, A. J. Neukirch, G. Gupta, J. J. Crochet, M. Chhowalla, S. Tretiak, M. A. Alam, H.-L. Wang and A. D. Mohite, *Science*, 2015, **347**, 522.
27. Y. Shao, Z. Xiao, C. Bi, Y. Yuan and J. Huang, *Nat. Commun.*, 2014, **5**, 5784.
28. C. W. Schlenker, K.-S. Chen, H.-L. Yip, C.-Z. Li, L. R. Bradshaw, S. T. Ochsenbein, F. Ding, X. S. Li, D. R. Gamelin, A. K. Y. Jen and D. S. Ginger, *J. Am. Chem. Soc.*, 2012, **134**, 19661.
29. A. Rao, P. C. Y. Chow, S. Gelinas, C. W. Schlenker, C.-Z. Li, H.-L. Yip, A. K. Y. Jen, D. S. Ginger and R. H. Friend, *Nature*, 2013, **500**, 435.
30. P. C. Y. Chow, S. Albert-Seifried, S. Gélinas and R. H. Friend, *Adv. Mater.*, 2014, **26**, 4851.

MH-COM-02-2015-000026 - Modulate Hybrid Organic–Perovskite Photovoltaic Performance by Controlling the Excited Dynamics of Fullerenes

Conceptual insights

Recent developments demonstrated that perovskite photovoltaics can be well built with an inorganic/organic p-i-n planar heterojunction architecture, in which organics interface with the perovskite. Across this heterointerface between two distinct material classes, efficient extraction of photogenerated charge carriers needs to be fulfilled in determining efficient device operation. One piece of absent chemical and physical pictures associated with these is how the organic functionalities control the properties of such heterointerface. This report presents a synergistic approach to modulate organic-perovskite interfaces and their corresponding photovoltaic behaviors by tuning the properties of n-contact fullerene layered atop of perovskite. The integrative chemistry, device, computational and spectroscopic studies show fullerene with excited charge transfer (CT) characteristics competes with singlet exciton decay and counteracts the excitonic nature associated with regular organic semiconductors. An important correlation is elucidated that shows the increase of excited CT probabilities between the fullerene and triphenylamine functionalities of n-layer organic contacts results in optimized interface and device operation of perovskite photovoltaics, with photocurrent enchantment and elimination of device hysteresis. This study provides a conceptually innovative model and indentifies material knobs to uncover the fundamental factors of organic-inorganic hybrid electronics.

Toc:

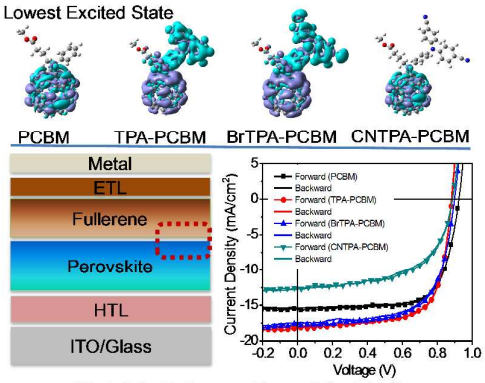

Text Abstract:

Fullerene with excited charge-transfer counteracts the excitonic nature of regular organics that results in improving perovskite-fullerene contact and photovoltaic performance.